18th International Conference on Information Fusion
Washington, DC - July 6-9, 2015

Individuals Motion Models Based on Probabilistic Distribution Profiles

Victor B. Frencl and João B. R. do Val
Faculty of Electrical and Computing Engineering
University of Campinas
Campinas, São Paulo, Brazil 13083-852
Emails: {frencl,jbosco}@dt.fee.unicamp.br

***Abstract*—The motion models of individuals should mathematically describe, as well as possible, the movements executed by an individual when he is walking, running or even stopping. There are some references in the literature with respect to individuals motion models, but most of them are based on image processing. In this paper, we proposed three probabilistic distribution profiles that can model the heading angle of an individual trajectory without relying on image processing. These profiles are based on probability density functions and cumulative distribution functions. Objectivity tests and standard deviation analysis were made in order to verify each profile behavior.**

I. Introduction

In target tracking problems, aircrafts [1] and ground vehicles [2] have well defined and categorized motion behaviors. For example, when an aircraft will perform a curve, it tilts its wings slowly inside the curve, executes the movement and exits the curve to return to a rectilinear trajectory. For ground vehicles, it is possible to observe its own motion behaviors. For example, when a ground vehicle will perform a curve, it slows down when it approaches the curve, executes the movement and exits the curve to return to a rectilinear trajectory.

When the object to track is not an aircraft or ground vehicle, but an individual walking or running, the situation is completely different as the motion behavior can be more erratic then aircrafts and ground vehicles. When observing individuals walking, several situations may occur in its trajectory: instant stops, walking on winding trails etc. Note that the movements of an individual have a lower inertia than aircrafts and ground vehicles.

In the literature, there are some works about motion models for individuals, but most of them are based on/combined with image processing methods. For example, in [3], it is proposed a method to obtain the number of individuals combining tracking methods and image processing. In [4], it is proposed combining image processing methods with behavioral models, whose mathematical structure is very complex. In [5], the objective is to track individuals in high density crowd based on the crowd images pixels.

Also in the literature, there are some studies about crowd disasters based on the individuals behaviors. In [6], a cognitive science approach was proposed, which is based on a behavioral heuristics model applied for the Love Parade crowd disaster [7]. This model predicts the emergence of self-organization phenomena, such as the spontaneous formation of unidirectional lanes or stop-and-go waves. Moreover, the combination of pedestrian heuristics with body collisions generates crowd turbulence at extreme densities. However, this model is very complex because is not only based on image processing but also based on a large set of complex collective dynamics.

Simple motion models can also be found in the literature. In [8], the directional process noise (DPN) model for ground targets is used. This model deals with different process noise variances for off-road (x and y directions) and on-road targets (orthogonal and "along the road" directions). In [9], an initial study of the individuals motion models can be found, where a simple mathematical model for individuals motions is used as the dynamic model for the GM-PHD filter in the target tracking problem.

Thus, in the present paper, some motion models proposals will be presented, whose objective is to reproduce individuals movements in a most plausible way without relying on image processing. These proposals envolve the heading angle probabilistic profiles, which aim is to create more realistic movements based on individuals walking and running. Three heading probabilistic profiles were proposed: the "drop", the "leaf" and the "balloon" profiles. These names come from the fact that they have similar shapes to a water drop, a plant leaf and a balloon, respectively.

At the end, an objectivity test will be applied to each of the proposals, in order to analyze the behavior of each profile and relating with their respective parameters. This objectivity test can classify more focused individuals or more dispersed behavior, with respect to its final destination.

II. Probabilistic Distribution Profiles

The probabilistic profiles have a different point of view with respect to image-based models, as in [10]. These image-based models generally use videos and image processing methods in order to obtain models for individuals movements. The idea of the probabilistic profiles proposed in this paper is to obtain plausible dynamic mathematical models for people trajectories. This can be very useful for target tracking in radar systems, from the point of view of state estimation. The corresponding dynamic model in the built-in radar stochastic filter can benefit from these probabilistic profiles.

The probabilistic profile of an individual motion is based on the heading angle α of the motion. This angle brings the information of the direction in which the individual is moving. These profiles are based on cumulative distribution functions and probability density function (pdf) of the orientation (heading angle). The three proposed profiles here are the "drop", the "leaf" and the "balloon" profiles.

A. "Drop" profile

The "drop" profile can be understood from the orientation diagram on Figure 1, which shows a motion to the north and it corresponds to the direction aligned to the individual orientation in some time instant. The vectors, which have the central point as the origin (individual position) and go toward the "drop" contour, represent the possible directions for which he may go. Each of the vectors magnitudes is directly proportional to the probability of this individual go to that corresponding direction. Therefore, the higher the vector magnitude is, the higher the probability of the individual go to the corresponding direction will be.

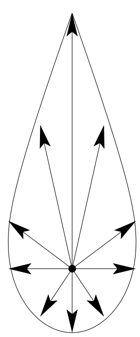

Fig. 1. Probabilistic profile – "Drop".

This profile can also be constricted, depending on the degree of objectivity in the movement. If an individual movement is more objective, the spatial distribution of his heading becomes more elongated since he tends to be less inclined to change his path at random. Conversely, the stretching in the heading distribution along the present heading is reduced in the observation of a more "distracted" walking. The more objective the individual, the thinner the profile and the probabilities of changing to a different direction becomes unlikely. The "drop" profile deformations are shown in Figure 2; note that when the objectivity becomes null (e.g., when an individual is stopped), the profile turns into a circumference.

1) Probability distribution: In order to be useful, three basic elements are defined, as follows:

- Choice of the probability density function $f_A(\alpha)$
- Determination of the cumulative distribution function $p_A(\alpha)$
- Calculation of the instantaneous heading angle α using the inverse function $\alpha = p_A^{-1}(u)$

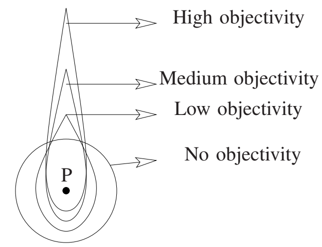

Fig. 2. "Drop" profiles for one direction with several objectivities.

Considering these steps, first we must choose a pdf $f_A(\alpha)$ in a way that the heading angle α has a profile similar to a water drop. The choice is made, as follows:

$$f_A(\alpha) = \frac{a}{2(a|\alpha| + 1)\ln(\gamma)}, \alpha \in [-\pi,\pi] \tag{1}$$

where $a \in \mathbb{R}$ and $\gamma \in \mathbb{R}$, $\gamma > 1$.

Now, taking into account appropriate intervals for α, i.e., $\alpha \in [-\pi,0]$ and $\alpha \in [0,\pi]$,

- $-\pi \leq \alpha < 0$:

$$\int_{-\infty}^{\alpha} f_A(t)dt = \frac{1}{2}\log_\gamma\left(\frac{1+a\pi}{1-a\alpha}\right) \tag{2}$$

- $0 \leq \alpha \leq \pi$:

$$\int_{-\infty}^{\alpha} f_A(t)dt = \frac{1}{2}\log_\gamma\left((1+a\pi)(1+a\alpha)\right) \tag{3}$$

Therefore:

$$p_A(\alpha) = \begin{cases} \frac{1}{2}\log_\gamma\left(\frac{1+a\pi}{1-a\alpha}\right) & , \quad \text{if } \alpha \in [-\pi,0) \\ \frac{1}{2}\log_\gamma\left((1+a\pi)(1+a\alpha)\right) & , \quad \text{if } \alpha \in [0,\pi] \end{cases} \tag{4}$$

To obtain the constant a in (4), we calculate $p_A(\alpha)$ at $\alpha = \pi$.

$$p_A(\alpha)|_{\alpha=\pi} = 1 \Rightarrow a = \frac{\gamma - 1}{\pi} \tag{5}$$

In Figure 3, the pdf was plotted for $\gamma = 1.5, \pi, 5, 10$.

In order to check the drop shape from the density given in (1), the plot of the pdf from the polar point of view is shown in the next plot. In Figure 4, there are four "drop" profiles for the values for γ used before.

For simulation purposes, the third and last step involves the calculation of the α angle from the inverse function $p_A^{-1}(u)$, where u is a random variable with uniform distribution, i.e., $\mathcal{U}(0,1)$. Thus, we have:

- If $0 \leq u < 0.5 (\equiv -\pi \leq \alpha < 0)$:

$$\alpha(u) = \pi\frac{1-\gamma^{1-2u}}{\gamma - 1} \tag{6}$$

- If $0.5 \leq u \leq 1.0 (\equiv 0 \leq \alpha \leq \pi)$:

$$\alpha(u) = \pi\frac{\gamma^{2u-1}-1}{\gamma - 1} \tag{7}$$

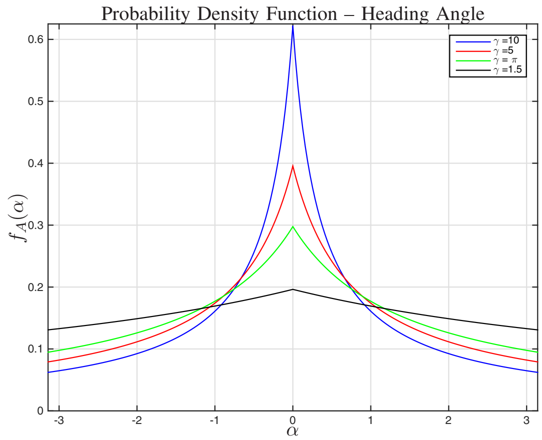

Fig. 3. Probability density function – “drop” profile.

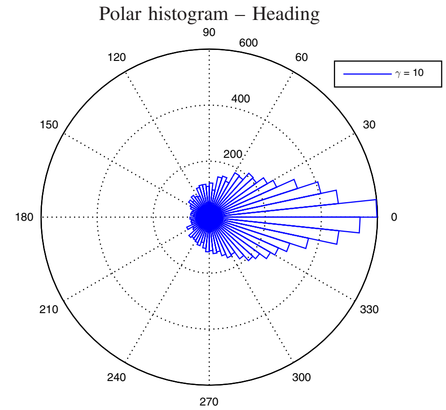

Fig. 5. “Drop” profile: polar histogram for heading angle.

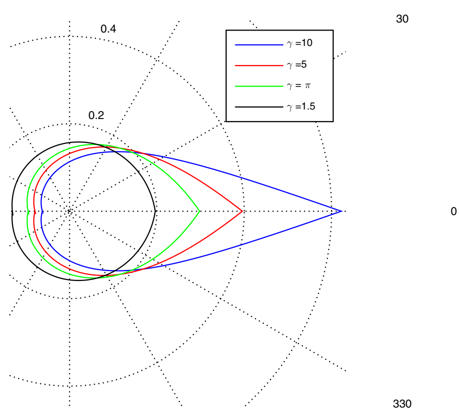

Fig. 4. “Drop” distribution profiles – polar format.

Therefore:

$$\alpha(u) = \begin{cases} \pi \dfrac{1-\gamma^{1-2u}}{\gamma - 1} & , \quad \text{if } u \in [0{,}0.5) \\[2ex] \pi \dfrac{\gamma^{2u-1}-1}{\gamma - 1} & , \quad \text{if } u \in [0.5{,}1.0] \end{cases} \tag{8}$$

Based on the equation (8), a polar histogram was created, in order to observe how the values for the heading angle behave. Figure 5 shows the mentioned polar histogram for the “drop” profile for $\gamma = 10$, 10,000 replications and 60 histogram bins.

Note that the histogram bins reflect the “drop” profile as expected. It is possible to observe that equation (8) can model well the randomness of the motion in a trajectory. This is allowed by the “drop” distribution.

B. “Leaf” profile

The “leaf” profile can be analyzed from the orientation diagram on Figure 6. The vectors, which have the central point as the origin (individual position) and go toward the “leaf” contour, represent the possible directions in which the individual may go. Each of the vectors magnitudes is directly proportional to the probability of this individual go to that corresponding direction, as in the “drop” profile.

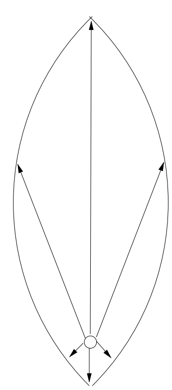

Fig. 6. Probabilistic profile – “Leaf”.

This profile can also be stretched or compressed, depending on the objectivity in which the individual moves, similarly to the “drop” profile, as illustrated in Figure 2.

1) Probability distribution: As in the “drop” profile, the determination of the “leaf” profile is based on the same three steps listed in Section II-A1.

First we have to choose a pdf $f_A(\alpha)$ for the heading angle in a way that it has a similar shape of a plant leaf. The choice is made based on the following pdf:

$$f_A(\alpha) = c\lambda e^{-\lambda|\alpha|}, \alpha \in [-\pi,\pi] \tag{9}$$

The next step is the determination of the cumulative distribution function on appropriate intervals for the angle α, i.e., $\alpha \in [-\pi,0]$ and $\alpha \in [0,\pi]$.

- $-\pi \leq \alpha < 0$:

$$\int_{-\infty}^{\alpha} f_A(t)dt = c(e^{\lambda\alpha} - e^{-\lambda\pi}) \tag{10}$$

- $0 \leq \alpha \leq \pi$:

$$\int_{-\infty}^{\alpha} f_A(t)dt = c\left(2 - e^{-\lambda\pi} - e^{-\lambda\alpha}\right) \tag{11}$$

Therefore:

$$p_A(\alpha) = \begin{cases} c(e^{\lambda\alpha} - e^{-\lambda\pi}) & , \quad \text{if } \alpha \in [-\pi,0) \\ c\left(2 - e^{-\lambda\pi} - e^{-\lambda\alpha}\right) & , \quad \text{if } \alpha \in [0,\pi] \end{cases} \tag{12}$$

In order to determine the constant c in (12), we calculate $p_A(\alpha)$ at $\alpha = \pi$, yielding:

$$c = \frac{1}{2\left(1 - e^{-\lambda\pi}\right)} \tag{13}$$

In Figure 7, the pdf given in equation (9) is shown for four values of $\lambda = 0.9, 1, \pi, 5$.

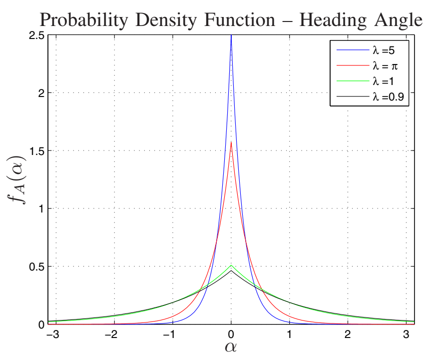

Fig. 7. Probability density function – "Leaf" profile.

Figure 8 shows the polar format of the pdf for the same values of λ.

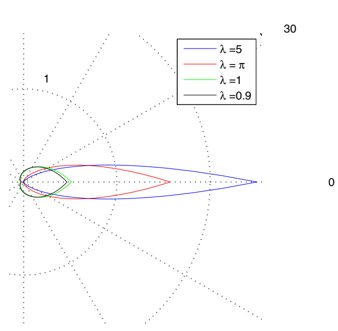

Fig. 8. "Leaf" distribution profiles – polar format.

Note that the shape of the polar distribution in Figure 8 looks like a plant leaf. It is possible to notice that the "leaf" profile is more elongated when compared with the drop profile, which brings more objectivity to the individual motion. Also, note that the parameter λ has the same effect as the parameter γ from the "drop" profile, from the point of view of objectivity.

For simulation purposes, the heading angle is calculated using the inverse function of the cumulative distribution function $p_A^{-1}(u)$, where $u \sim \mathcal{U}(0,1)$. Considering the constant c from the equation (13), we have the following:

- If $0 \leq u < 0.5 (\equiv -\pi \leq \alpha < 0)$:

$$\alpha(u) = \frac{1}{\lambda} \ln\left(\frac{u + ce^{-\lambda\pi}}{c}\right) \tag{14}$$

- If $0.5 \leq u \leq 1.0 (\equiv 0 \leq \alpha \leq \pi)$:

$$\alpha(u) = \frac{1}{\lambda} \ln\left(\frac{c}{2c - (u + ce^{-\lambda\pi})}\right) \tag{15}$$

Therefore:

$$\alpha(u) = \begin{cases} \frac{1}{\lambda} \ln\left(\frac{u + ce^{-\lambda\pi}}{c}\right) & , \quad \text{if } u \in [0,0.5) \\ \frac{1}{\lambda} \ln\left(\frac{c}{2c - (u + ce^{-\lambda\pi})}\right) & , \quad \text{if } u \in [0.5,1.0] \end{cases} \tag{16}$$

Based on the equation (16), a corresponding polar histogram was created, in order to observe how the values for the heading angle behaves. Figure 9 shows the mentioned polar histogram for the "leaf" profile for $\lambda = 3$, 10,000 replications and 60 histogram bins.

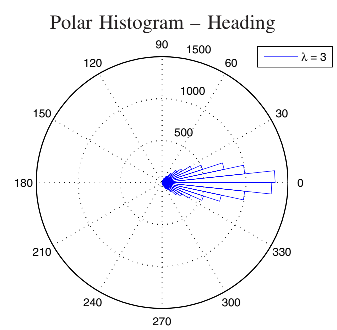

Fig. 9. "Leaf" profile: polar histogram for heading angle.

Note that the histogram bins resemble the "leaf" profile as expected. It is possible to observe that the equation (16) shows the randomness of the motion in a trajectory. This is allowed by the "leaf" distribution.

C. *"Balloon" profile*

The "balloon" profile is the most simple among the proposed profiles because it is based on a zero-mean gaussian distribution. Its pdf and cdf is given by:

$$f_A(\alpha) = \frac{1}{\sigma\sqrt{2\pi}} \exp\left(-\frac{\alpha^2}{2\sigma^2}\right) \tag{17}$$

$$p_A(\alpha) = \frac{1}{2}\left[1 + \text{erf}\left(\frac{\alpha}{\sigma\sqrt{2}}\right)\right] \tag{18}$$

where

$$\text{erf}(x) = \frac{1}{\sqrt{\pi}} \int_{-x}^{x} e^{-t^2} dt \tag{19}$$

is the error function. In Figure 10, it is shown the polar format for the pdf for four values of $\sigma = 0.45, 0.55, 0.65, 0.75$.

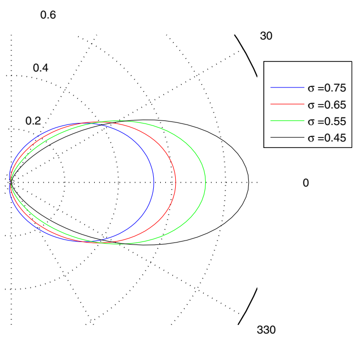

Fig. 10. "Balloon" distribution profiles – polar format.

Note that the cdf $p_A(\alpha)$ depends on the error function, which does not allow to obtain the inverse function $p_A^{-1}(u)$ analytically. As this step has the purpose of simulating, the inverse function will be determined considering the $y = \text{erf}(x)$ and $x = \text{erf}^{-1}(y)$ functions, commonly found and implemented in mathematical softwares, such as Matlab, and therefore can be calculated numerically in simulations:

$$\alpha(u) = \text{erf}^{\ -1}(2u - 1)\sqrt{2}\sigma \tag{20}$$

where u is a random variable with uniform distribution, i.e., $\mathcal{U}(0,1)$.

Based on the equation (20), a polar histogram was created, in order to observe how the values for the heading angle behave. Figure 11 shows the mentioned polar histogram for the "balloon" profile for $\sigma = 1$, 10,000 replications and 60 histogram bins.

Note that the histogram bins are more spread out around the heading of the individual. This is a more flat profile at its peak providing some degrees of motion for left and right.

III. Objectivity Test

Based on the probabilistic profiles proposed in the previous sections, tests will be applied on these profiles to verify the behavior in regards to the objectivity of each profile.

The objectivity characteristic is directly linked to the parameters of each probabilistic profile: γ for the "drop" profile, λ for the "leaf" profile and σ for the "balloon" profile. It will be analyzed the behavior of a simple trajectory, based on these parameters.

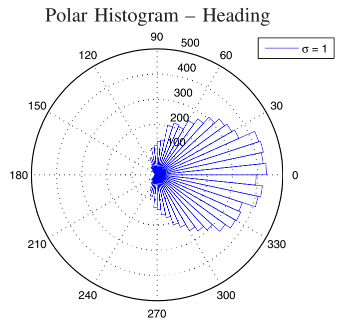

Fig. 11. "Balloon" profile: polar histogram for heading angle.

To perform the objectivity test, a simple bidimensional scenario was created. In these scenarios, a single individual is generated over the magenta point at the center and walks freely through the green zone until it reaches the black region, where the trajectory ends. For both profiles, we adopted an average speed with a magnitude of 1.5m/s and a standard deviation of 0.5m/s around the average speed.

A. "Drop" profile

The first test takes into account the "drop" profile (Section II-A). Figure 12 shows the trajectories for $\gamma = 10$ and $\gamma = 100$. The small arrows represent the velocity vector and they contain the heading angle information.

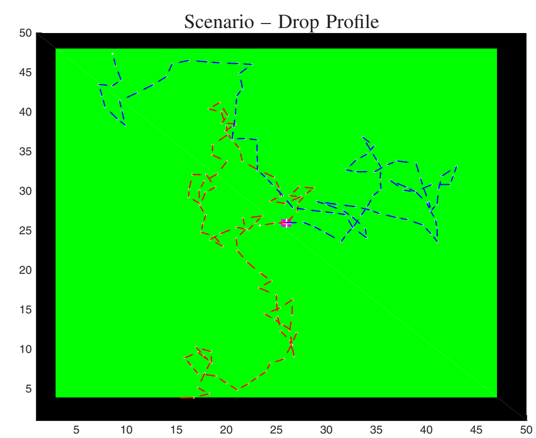

Fig. 12. Trajectories using "drop" profile (red arrows: $\gamma = 10$; blue arrows: $\gamma = 100$).

It is interesting to observe that the trajectories have similar objectivity behavior, even when the parameter γ was changed by a multiplicative factor of 10.

B. "Leaf" profile

The second test takes into account the "leaf" profile (Section II-B). Figure 13 shows the trajectory for $\lambda = 2$ and $\lambda = 5$. The small arrows represent the velocity vector and they contain the heading angle information.

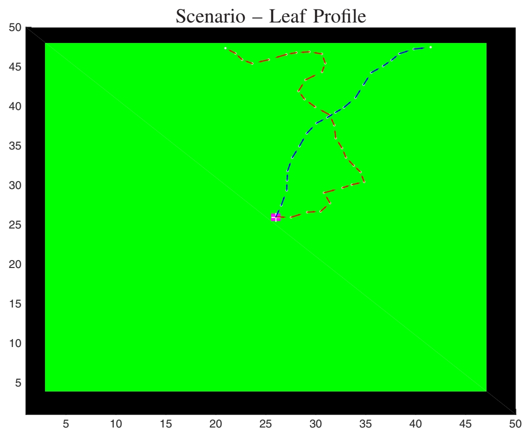

Fig. 13. Trajectories using "leaf" profile (red arrows: $\lambda = 2$; blue arrows: $\lambda = 5$).

Differently from the "drop" profile, the two trajectories have distinct behaviors. For $\lambda = 2$, the trajectory changes considerably along its path. In the case $\lambda = 5$, the trajectory features a more objective behavior in regards to the motion direction towards the final destination.

C. "Balloon" profile

The third and last test takes into account the "balloon" profile. Figure 14 shows the trajectory for $\sigma = 0.1$ and $\sigma = 1.0$. The small arrows represent the velocity vector and they contain the heading angle information.

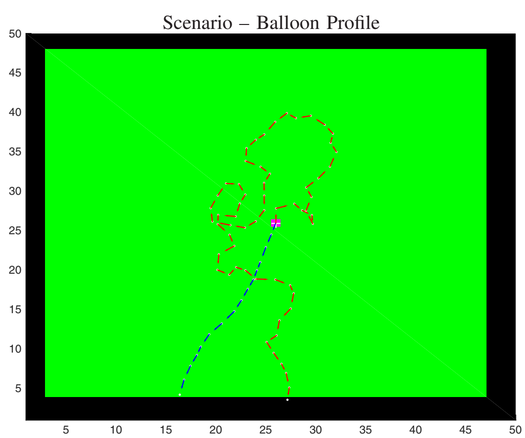

Fig. 14. Trajectories using "balloon" profile (red arrows: $\sigma = 1.0$; blue arrows: $\sigma = 0.1$).

The third case presents the following behavior: for $\sigma = 0.1$, the trajectory is very objective with respect to its the final destination. For $\sigma = 1.0$, the trajectory becomes more adrift. Note that the individual objectivity is inversely proportional to the σ parameter: the greater the variance, the greater the variability of trajectory and vice versa. The "balloon" profile can be modeled directly by a gaussian distribution, bringing a special appeal to the point of view of stochastic filtering based on noises with gaussian distribution.

D. Standard deviation analysis

In order to verify the influence of the parameters γ, λ and σ on the variability of the trajectories, we analyzed the heading angle random variable standard deviations[1] as a function of $1/\gamma$, $1/\lambda$ and σ.

The standard deviation for the "drop" profile can be calculated using the pdf $f_A(\alpha)$ in equation (1) and the standard deviation definition (assuming zero-mean random variable):

$$\sigma_{\text{drop}}(\gamma) = \sqrt{\int_{-\pi}^{\pi} \alpha^2 \frac{a}{2(a|\alpha| + 1)\ln(\gamma)} d\alpha}, \quad a = \frac{\gamma - 1}{\pi} \tag{21}$$

Note that the integral in equation (21) is not analytical and, the analysis of this standard deviation will be on the numerical point of view.

For the "leaf" profile, the standard deviation can be obtained as follows:

$$\sigma_{\text{leaf}}(\lambda) = \sqrt{\int_{-\pi}^{\pi} \alpha^2 c\lambda e^{-\lambda|\alpha|} d\alpha}, \quad c = \frac{1}{2(1 - e^{-\lambda\pi})} \tag{22}$$

Calculating the integral in (22), we obtained the following result (as a function of λ):

$$\sigma_{\text{leaf}}(\lambda) = \sqrt{-\frac{\pi^2\lambda^2 + 2\pi\lambda - 2e^{\lambda\pi} + 2}{\lambda^2(e^{\lambda\pi} - 1)}} \tag{23}$$

Figure 15 shows the standard deviation as a function of $1/\gamma$, $1/\lambda$ and σ. For the integral in (21), we used the Wolfram Alpha tool [11]. The website provides several mathematical calculations both numeric and analytical. Using the Wolfram Alpha tool, we calculated 15 values of σ_{drop} for 15 values of γ: $\gamma = 1.01, 1.5, 2, 10, 20, 30, 50, 70, 100, 150, 200, 250, 300, 350, 400$ (note that $1/\gamma < 1$; see eq. (1)).

Note from the plots on Figure 15 that the "drop" standard deviation is always greater than σ_{leaf} and σ_{balloon}. This plot shows what was seen on Figure 12, i.e., the lack of objectivity of the trajectories originated from the "drop" profile, whereas, it can also be seen that the smaller the parameter λ, the greater the standard deviation and, from $1/\lambda = \sigma = 1.25$, the σ_{leaf} is always lower than σ_{balloon}.

E. Trajectory model

In the simulations presented in Sections III-A, III-B and III-C, it was used a trajectory model based on the time evolution of six elements of the state vector: the position

[1]The standard deviation parameter σ works as a reference for the other two parameters.

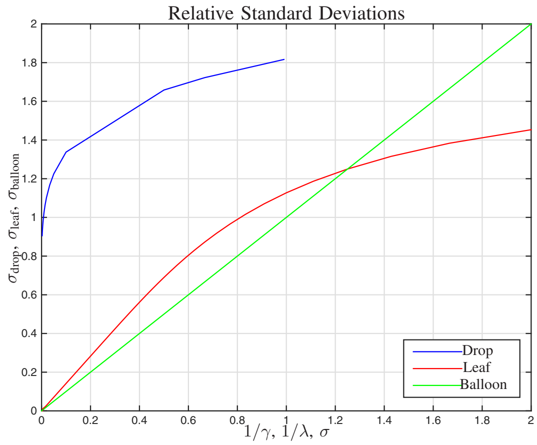

Fig. 15. Standard deviations $\times$ $\{1/\gamma,\, 1/\lambda,\, \sigma\}$.

components (x_k,y_k), the velocity components (s_k^x,s_k^y), the speed (s_k) and heading angle (α_k).

The position and velocity components are determined based on a constant velocity motion. Considering that $\mathbf{p}_k = [x_k\ y_k]^T$ and $\mathbf{s}_k = [s_k^x\ s_k^y]^T$, we have:

$$\mathbf{p}_{k+1} = \mathbf{p}_k + s_k dT \begin{bmatrix} \cos(\alpha_k) \\ \sin(\alpha_k) \end{bmatrix} \tag{24}$$

$$\mathbf{s}_{k+1} = \frac{\mathbf{p}_{k+1} - \mathbf{p}_k}{dT} = s_k \begin{bmatrix} \cos(\alpha_k) \\ \sin(\alpha_k) \end{bmatrix} \tag{25}$$

where dT is the sampling time.

The speed component is evaluated based on the average speed of an individual i ($\bar{s}_i$) and its standard deviation (σ_{s_i}). These values are predetermined in the simulation. So, we have:

$$s_k = \bar{s}_i \pm \sigma_{s_i} u_1 \tag{26}$$

where u_1 is a random variable based on some distribution with zero mean.

Finally, the heading angle α_k evolves according with the following expression:

$$\alpha_{k+1} = \alpha_k + \alpha(u_2) \tag{27}$$

where $u_2 \sim \mathcal{U}(0,1)$ and $\alpha(u_2)$ is given by equation (8) or (16), depending on the chosen profile (“drop” or “leaf”).

It is possible to express equations (24)–(27) in a matrix notation, as follows:

$$\mathbf{x}_{k+1} = A\mathbf{x}_k + \mathbf{b} \tag{28}$$

where

$$\mathbf{x}_k = \begin{bmatrix} x & y & s^x & s^y & s & \alpha \end{bmatrix}_k^T \tag{29}$$

$$A = \begin{bmatrix} 1 & 0 & 0 & 0 & \cos(\alpha_k)dT & 0 \\ 0 & 1 & 0 & 0 & \sin(\alpha_k)dT & 0 \\ 0 & 0 & 0 & 0 & \cos(\alpha_k) & 0 \\ 0 & 0 & 0 & 0 & \sin(\alpha_k) & 0 \\ 0 & 0 & 0 & 0 & 0 & 0 \\ 0 & 0 & 0 & 0 & 0 & 1 \end{bmatrix} \tag{30}$$

$$\mathbf{b} = \begin{bmatrix} 0 & 0 & 0 & 0 & \bar{s}_i \pm \sigma_{s_i} u_1 & \alpha(u_2) \end{bmatrix}^T \tag{31}$$

Figure 16 shows an example of a scenario with a high number of individuals moving around, which can be employed on radar surveillance studies. The colors that appear in this scenario represents several types of terrains (easy to walk terrains – blue, difficult to walk terrains – yellow, insurmountable obstacles – red). In this case, the direction of each trajectory is modeled by the “leaf” profile. The general behavior presents a good resemblance to real movement of individuals. In this scenario, the “leaf” profile was primarily used to generate the trajectories, combined with elements that restrict the free movement.

Some brief details about how the trajectories behave in the scenario with obstacles are provided. The trajectories are generated at magenta points. When a trajectory is generated, its final destination is already defined from the begining (towards the black region). The trajectory is guided by the so-called subdestinations (cyan points). These subdestinations are previously defined in the scenario. When the trajectory find a subdestination, the new subdestination is calculated based on the preferred choice between the distance to its final destination and the nearest subdestinations; the one with the smallest distance is the chosen one. This is repeated until the trajectory arrives to its final destination, where the trajectory vanishes.

The different terrains have different probability values relative to change to a new direction to proceed. For example, an individual walking on the yellow terrain has a higher probability to stop and change the direction of the trajectory than on the blue terrain. The red obstacle is different: when the trajectory hits a red obstacle, a new direction is defined, acting like a wall. The green terrain is a free movement zone.

IV. Conclusion

In this paper, three types of probabilistic profiles were proposed. These profiles models the heading angle of trajectories of individuals and they are able to provide the direction in which an individual is moving. Each probabilistic profile is based on the definition of the cumulative distribution function and the probability density function of the random variable, which models the heading orientation of the walking movement of an individual. The “drop” profile provides a more erratic movement; the “leaf” profile gives a characteristic of greater objectivity to the individual, in relation to his final destination; the “balloon” profile has a more flat profile at its peak providing some degrees of motion for left and right. It

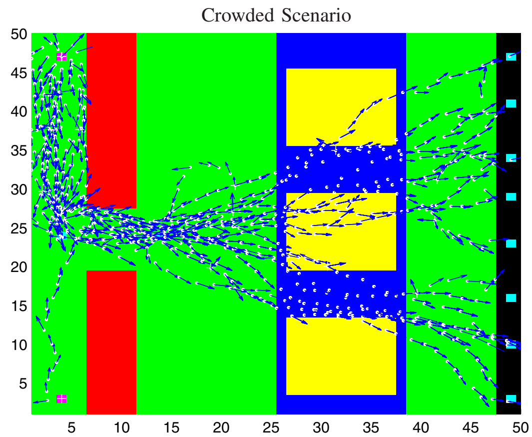

Fig. 16. Example of a scenario with a high number of trajectories.

was observed that the parameters γ, λ and σ are responsible for the objectivity of the individual.

For each probabilistic profile, a test was performed to verify the behavior of the model, as regards to the sensitivity of their adjustment parameters. Some interesting characteristics are observed. For example, the "drop" profile has a low sensitivity to changes in the value of γ, while the sensitivity of the "leaf" profile is reasonable, when the parameter λ is modified. The "balloon" profile objectivity is inversely proportional to the σ parameter. The influence of each parameter was evaluated by means of the standard deviation analysis with respect to the heading random variable.

Based on the results in Section III-A (objectivity test, standard deviation analysis), it is possible to conclude that the parameters γ, λ and σ in each profile are responsible for shaping the probabilistic heading behavior, with different sensitivity for each model. Furthermore, from the simulations, we observe that the trajectories can represent not only pedestrians walking/running (trajectories with small heading changes), but depending on the parameters, foraging animals or ants searching for food (trajectories with frequent heading changes). In both cases, the model can be inserted in structured scenarios with or without obstacles.

One possible extension of the models proposed here would be to apply them to target tracking problems, in order to observe the performance of the proposed probabilistic models in comparison with standard models, such as nearly-constant velocity model. There is also a possible extension of the profiles to the 3D space for aircrafts, UAVs or even birds. However it is necessary to verify its complexity since it must take into account not only the heading angle but also roll and pitch angles.

Acknowledgment

The authors would like to thank CNPq, Grant 303292/2010-5, and the Brazilian agency CAPES for financial support.

References

[1] X. R. Li and V. P. Jilkov, "Survey of maneuvering target tracking. part i. dynamic models," *IEEE Transactions on Aerospace and Electronic Systems*, vol. 39, no. 4, pp. 1333–1364, 2003.

[2] N. Cui, L. Hong, and J. R. Layne, "A Comparison of Nonlinear Filtering Approaches with an Application to Ground Target Tracking," *Signal Processing*, vol. 85, no. 8, pp. 1469–1492, 2005.

[3] G. Antonini and J. P. Thiran, "Counting pedestrians in video sequences using trajectory clustering," *IEEE Transactions on Circuits and Systems for Video Technology*, vol. 16, no. 8, pp. 1008–1020, 2006.

[4] G. Antonini, S. V. Martine, M. Bierlaire, and J. P. Thiran, "Behavioral priors for detection and tracking of pedestrians in video sequences," *International Journal of Computer Vision*, vol. 69, no. 2, pp. 159–180, 2006.

[5] S. Ali and M. Shah, "Floor fields for tracking in high density crowd scenes," in *10th European Conference on Computer Vision*, 2008.

[6] M. Moussad, D. Helbing, and G. Theraulaz, "How simple rules determine pedestrian behavior and crowd disasters," *Proceedings of the National Academy of Sciences*, vol. 108, no. 17, pp. 6884–6888, 2011. [Online]. Available: http://www.pnas.org/content/108/17/6884.abstract

[7] D. Helbing and P. Mukerji, "Crowd disasters as systemic failures: analysis of the love parade disaster," *EPJ Data Science*, vol. 1, no. 1, p. 7, 2012. [Online]. Available: http://www.epjdatascience.com/content/1/1/7

[8] T. Kirubarajan, Y. Bar-Shalom, K. Pattipati, and I. Kadar, "Ground target tracking with variable structure imm estimator," *Aerospace and Electronic Systems, IEEE Transactions on*, vol. 36, no. 1, pp. 26–46, Jan 2000.

[9] V. Frencl and J. do Val, "State estimation using gm-phd filter applied to the tracking of individuals," in *2013 IEEE Radar Conference (RADAR)*, April 2013, pp. 1–6.

[10] M. Andriluka, S. Roth, and B. Schiele, "People-tracking-by-detection and people-detection-by-tracking," in *IEEE Conf. on Computer Vision and Pattern Recognition (CVPR'08)*, June 2008, pp. 1–6.

[11] Wolfram alpha computational knowledge engine. [Online]. Available: www.wolframalpha.com